Supplementary Data

RHAMM (CD168)-Targeted Redox Responsive Hyaluronic Acid Nanogels for Treating Both Primary and Metastatic Tumors

Chenchen Yang, Cheng Li, Peng Zhang, Wei Wu and Xiqun Jiang✉

[1]Department of Polymer Science & Engineering, College of Chemistry & Chemical Engineering, Nanjing University, Nanjing 210023, P. R. China.

✉Corresponding authors: Xiqun Jiang.

Email: jiangx@nju.edu.cn

Experimental

Materials

Acryloyl chloride was purchased from Shanghai Chemical Reagent Co. (China). Hyaluronic acid (HA) (Mw = 7 kDa) was obtained from Freda Bio-chem. Co. Ltd (Shandong China). The recrystallized potassium persulfate ($K_2S_2O_8$) was used. Anti-CD44 antibody was obtained from Multi Sciences (Lianke) Biotech Co. Ltd. Anti-RHAMM antibody and fluorescein isothiocyanate (FITC) linked goat anti-rabbit immunoglobulin G (IgG) was obtained from Boster Biological Technology CO., Ltd (Wuhan, China). Doxorubicin hydrochloride (DOX), Methacrylic anhydride, Cystamine dihydrochloride, glutathione (GSH), *N, N'*- methylene bisacrylamide (MBA), NIR-797 isothiocyanate, FITC, rhodamine B isothiocyanate (RBITC), Hoechst 33258 and other reagents were of analytical grade. All organic solvents were dehydrated before used. LNCaP cell line (human prostate cancer), H22 cell line (Murine hepatic), A549 cell line (human pulmonary carcinoma), NIH3T3 cell line (murine embryonic fibroblast) and L-02 cell line (human normal liver) were purchased from Shanghai Institute of Cell Biology (Shanghai, China). All cell lines were maintained in RPMI-1640 (Gibco, Grand Island, USA) with 10% fetal bovine serum (FBS，Hyclone, Waltham, USA) and 1% Penicillin-Streptomycin Solution. Cells were incubated at 37 °C with 5% CO_2.

Synthesis of methacrylated hyaluronic acid (MAHA) and cystamine bisacrylamide (CBA)

1.0 g of sodium HA and 3 mL (19.96 mmol) of methacrylic anhydride were dissolved in 100 mL of de-ionized water at 0 °C. Then appropriate NaOH solution (1 M) was added to sustain the pH of the solution around 8. After reaction for 24 h, the solution was precipitated in ethanol and washed three times. At last, the white powder of MAHA was dried in vacuum oven overnight. The degree of substitution (DS) of the methacrylic molecules (MA) in HA was detected by ^{1}H NMR in deuterium oxide (D_2O). ^{1}H NMR (400 MHz, D_2O): δ 6.09 (s, 1H, C***H***H=CCH_3CO-), 5.68 (s, 1H, CH***H***=CCH_3CO-), 1.95 (s, 3H, NHCOC***H$_3$***) (Fig. S1). 5.6 g (36.36 mmol) of Cystamine dihydrochloride was dissolved in 20 mL of de-ionized water. NaOH solution (10 M, 20 mL) and acryloyl chloride (100 mmol) were then added dropwise synchronously at 0 °C for 24 h. Then the raw product was acquired by filtration and washed

three times using ice de-ionized water. The solid was purified by recrystallization with ethyl acetate. Finally, the white powder, CBA, was dried in vacuum oven (4.7 g, 73%) [1]. ^{1}H NMR (400 MHz, DMSO-*d6*): δ 8.31 (t, J = 5.3 Hz, 2H, -CON***H***CH2-), 6.22 (dd, J = 17.1, 10.1 Hz, 2H, CHH=C***H***CO-), 6.09 (dd, J = 17.1, 2.3 Hz, 2H, C***H***H=CHCO-), 5.60 (dd, J = 10.0, 2.3 Hz, 2H, CH***H***=CHCO-), 3.42 (dd, J = 12.8, 6.4 Hz, 4H, -NHC***H***2CH2-), 2.82 (t, J = 6.8 Hz, 4H, -CH2C***H***2S-) (Fig. S2).

Preparation and characterization of HA nanogels and DOX-loaded nanogels

Redox-responsive nanogels (HAss nanogels) were prepared by radical copolymerization of MAHA (Fig. S1) and CBA (Fig. S2). Firstly, MAHA (50 mg) and CBA (60 mg, 0.23 mmol) were added in 10 mL of de-ionized water. The polymerization was initiated by recrystallized potassium persulfate ($K_2S_2O_8$) at 81 °C and reacted for 40 min in nitrogen environment. At last, the HAss nanogels suspension was purified by dialyzing against de-ionized water (MWCO = 14 kDa) for 24 h. Similarly, MBA was applied to prepare HAcc nanogels which are insensitive to reductive environment with the same method as contrast. The hydrodynamic diameter and ζ-potential of HA nanogels was detected by dynamic light scattering (DLS) technique (Brookheaven Instruments Co., USA) and Zeta Potential Analyzer (Brookhaven Instruments Co., USA), respectively. Morphological characteristics of nanogels were operated on transmission electron microscope (TEM) (JEOL, Japan) (100 kV). The drug-loaded nanogels (DOX loaded HAss and HAcc) were prepared by mixing a HA nanogels suspension (3 mL, 5 mg/mL) with 1.4 mL of DOX solution (6 mg/mL), and the final pH was approximately 7.0. In order to enclose DOX into the nanogels matrix, the mixture was stirred in dark for 24 h at 37 °C. The resulting mixture was centrifuged with 16000 rpm for 90 min to separate the unloaded DOX and the exterior DOX from drug-loaded nanogels, and the sediment was re-dispersed in 10 mM phosphate buffered saline (PBS) (pH = 7.4, 150 mM NaCl). The amount of DOX in nanogels was measured by using UV/Vis spectrometry (UV-5300, Metash, China) (481 nm), and the weight of the DOX-loaded HA nanogels was acquired with vacuum drying overnight. The drug loading content (D.L.) was calculated as Equation S1 and encapsulation efficiency (E.E.) of the nanogels was calculated as Equation

S2.

D.L. (%) = (Mass of drug in nanogels)/(Mass of the drug loaded nanogels)×100% (S1)

E.E. (%) = (Mass of drug in nanogels)/(Total Mass of drug)×100% (S2)

Stability and release analysis of nanogels

1 mL (5 mg/mL) HAss nanogels were mixed in 30% FBS or bovine serum albumin (BSA) with different concentrations, and the light scattering intensity and hydrodynamic diameter of the samples were detected at 37 °C by DLS measurement.

In the reduction-triggered degradation experiment, 2 mL of HAss nanogels (5 mg/mL) were mixed with 1 mL of PBS (pH = 7.4) or PBS (pH = 7.4) containing 3 mM , 30 mM or 120 mM GSH at 37 °C. Similarly, the DLS data of each sample were acquired at predetermined period. The morphology photo of the GSH-treated sample was obtained by TEM. According to the previous work [2], in brief, DOX-loaded HAss nanogels was enclosed into a dialysis bag (MWCO = 14 kDa) with a known DOX concentration (0.9 mg/mL) and then placed into 5 mL of PBS (pH = 7.4, 5.0, respectively) or PBS (pH = 7.4, 5.0, respectively) containing 10 mM GSH at 37 °C. All the release PBS was collected and substituted with 5 mL of corresponding fresh PBS at predetermined period. The release behavior of DOX from HAcc nanogels with and without GSH at pH 7.4 was measured in the same way. All the release data were obtained by probing the absorbance at 481 nm with the UV/Vis spectrometry.

Cytotoxicity assays

In MTT assays, LNCaP, H22, A549 and NIH3T3 cell lines were applied and the L-02 cell line was utilized as a normal cell model for verifying the biocompatibility of HAss nanogels. All kinds of the cells were seeded in a 96-well plate at the density of 5000 cells per well with incubating for 24 h at 37 °C in cell incubator, respectively, and then 20 μL of free DOX, empty HAss nanogels and DOX-loaded HAss nanogels at prescribed concentrations were added into the medium and incubated for another 24 h in the same condition. Subsequently, the medium with drug was removed and each well was washed with PBS. Then 20 μL 3-(4, 5-dimethylthiazol-2-yl)-2, 5-diphenyltetrazolium bromide (MTT) solution (5

mg/mL) with 180 μL of complete medium were added into each well and incubated for 4 h. Then the medium was withdrawn and 150 μL dimethyl sulfoxide (DMSO) was added to obtain the formazan solution, the absorbance (570 nm) of each well was explored on a microplate reader (Huadong, DG-5031, China), HAcc nanogels were treated as the same method. The cell viability was calculated by Equation S3.

Cell Viability (%) = (The absorbance of test group)/(The absorbance of control group)×100% (S3)

Supplementary Figures

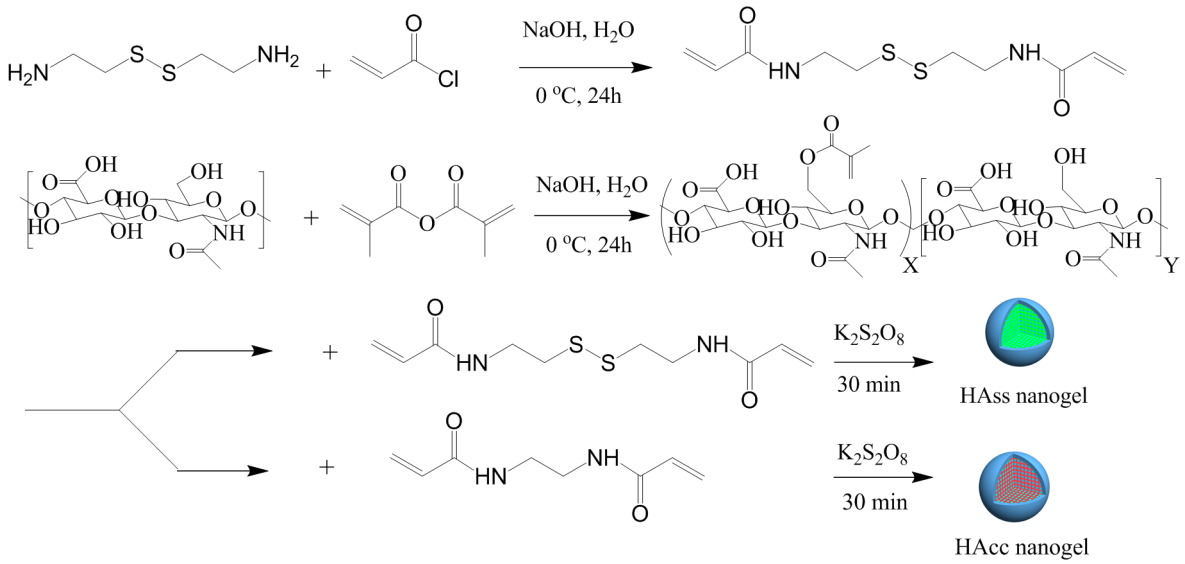

Scheme S1. The synthesis plots of HAss nanogels and HAcc nanogels.

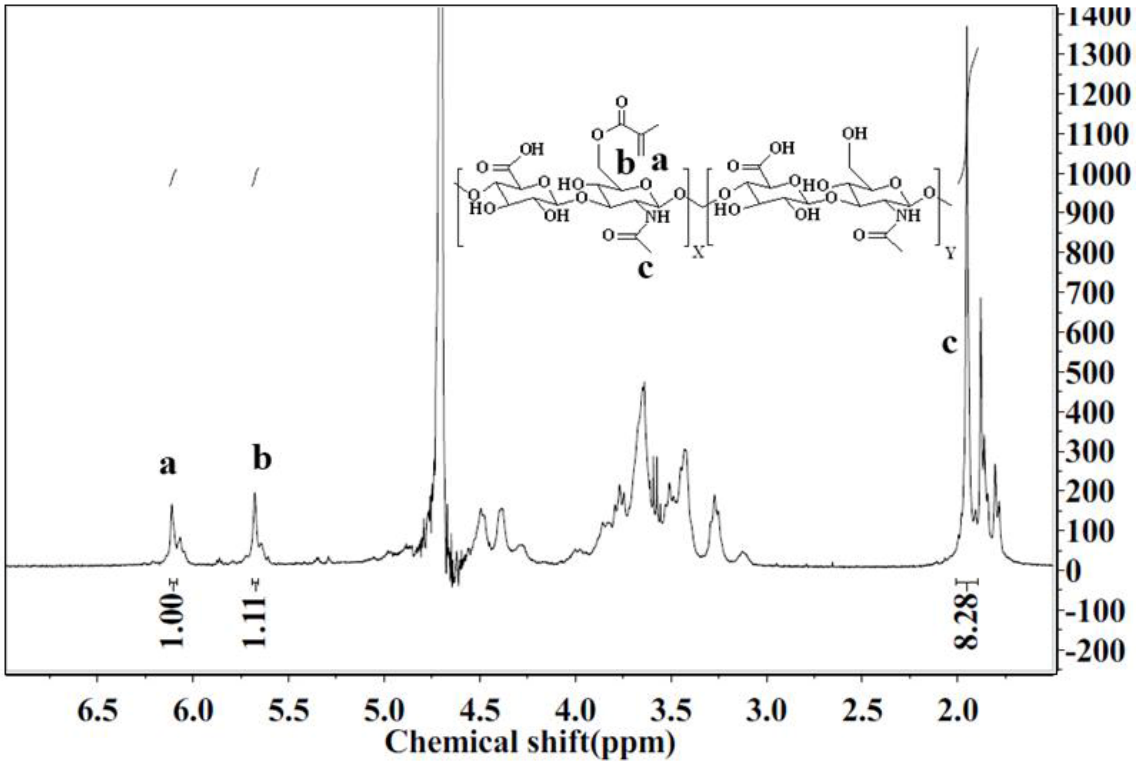

Fig. S1. ^{1}H NMR spectrum of MAHA in D_2O.

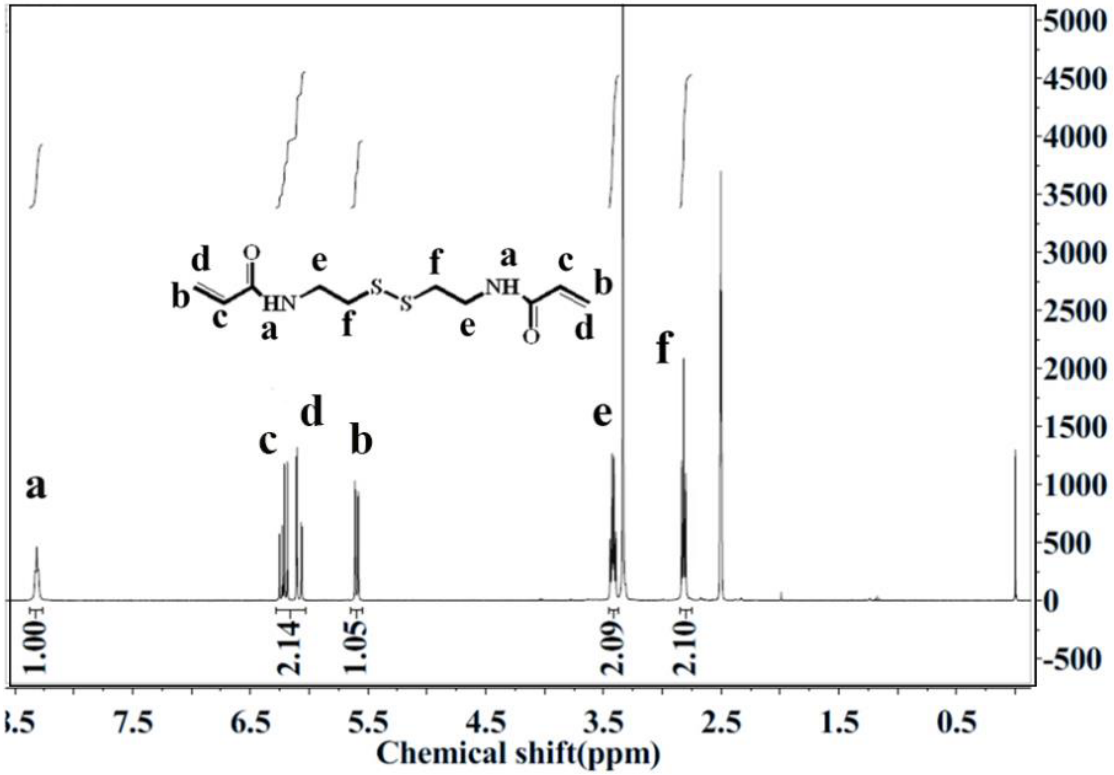

Fig. S2. ^{1}H NMR spectrum of CBA in DMSO-*d6*.

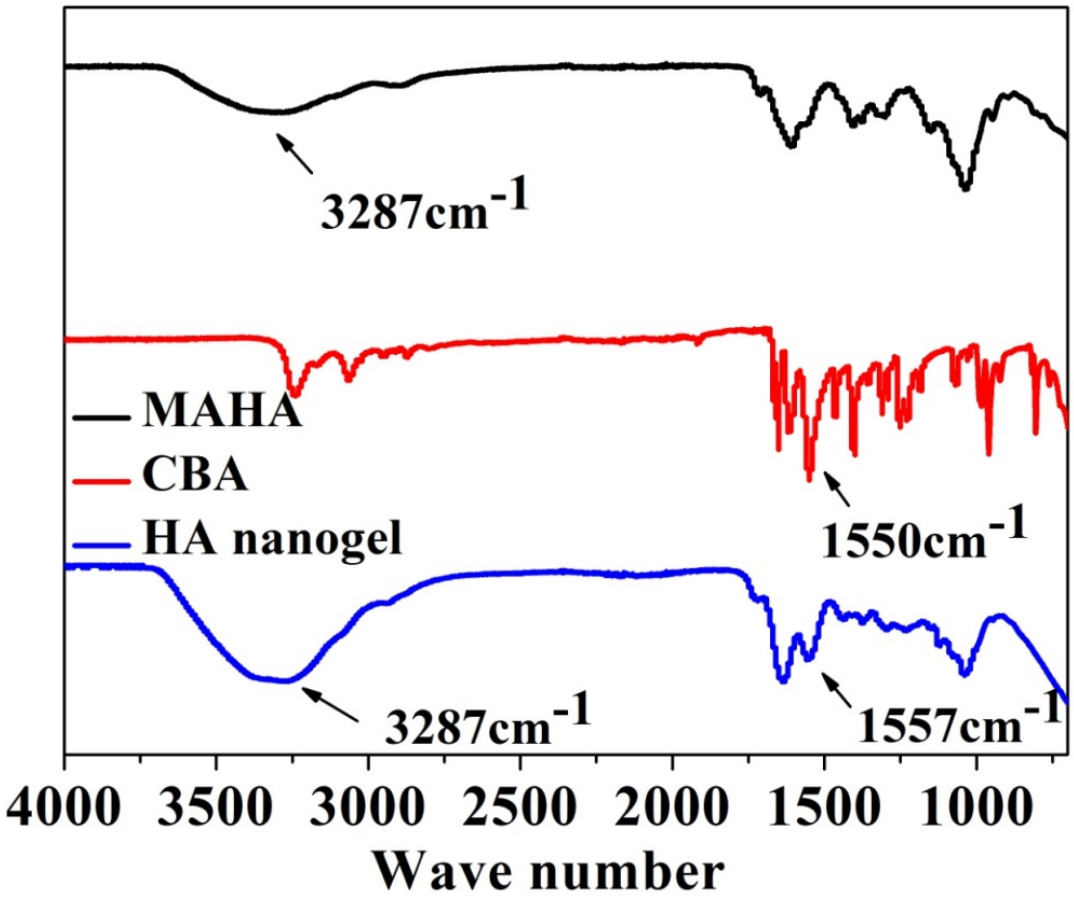

Fig. S3. The FT-IR spectra of MAHA (up), CBA (middle) and HAss nanogels (bottom).

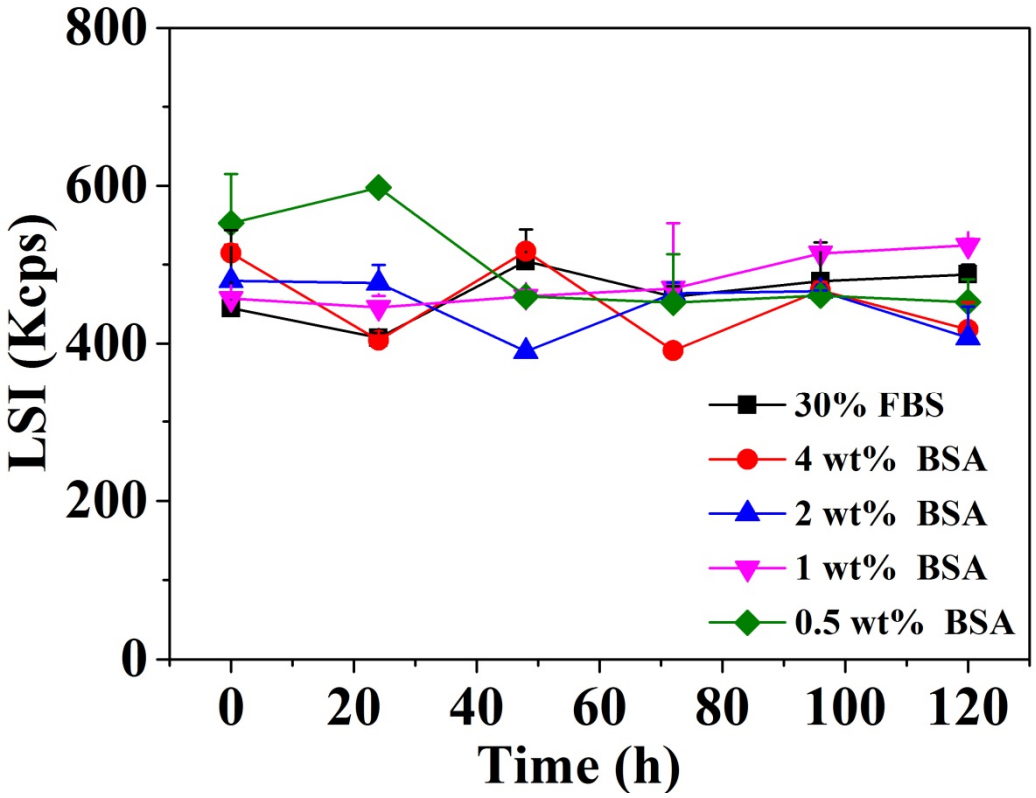

Fig. S4. The light scattering intensity (LSI) stabilities of HAss nanogels in FBS and BSA solutions (mean ± s.d., n = 3).

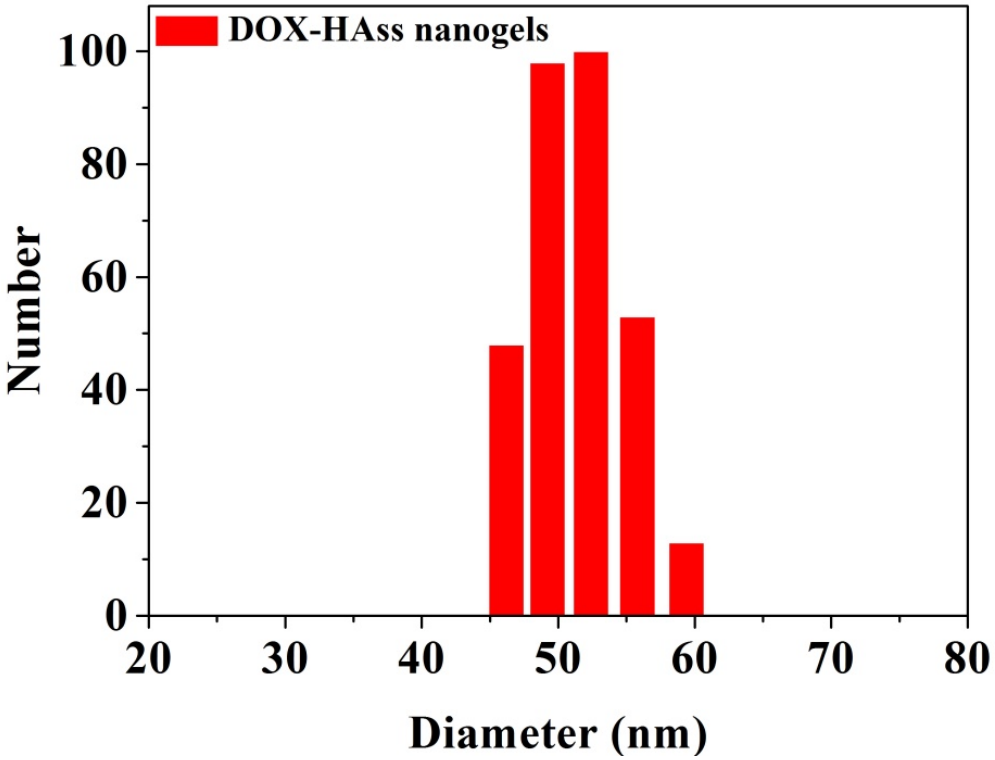

Fig. S5. The DLS plot of DOX-loaded HAss nanogels.

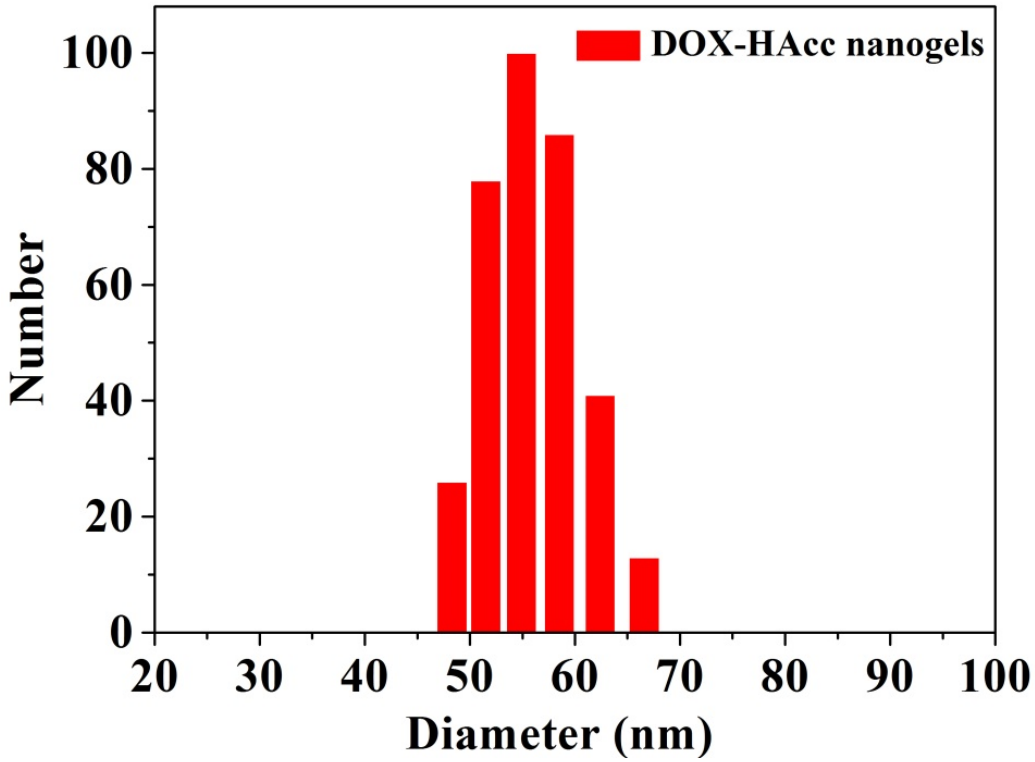

Fig. S6. The DLS plot of DOX-loaded HAcc nanogels.

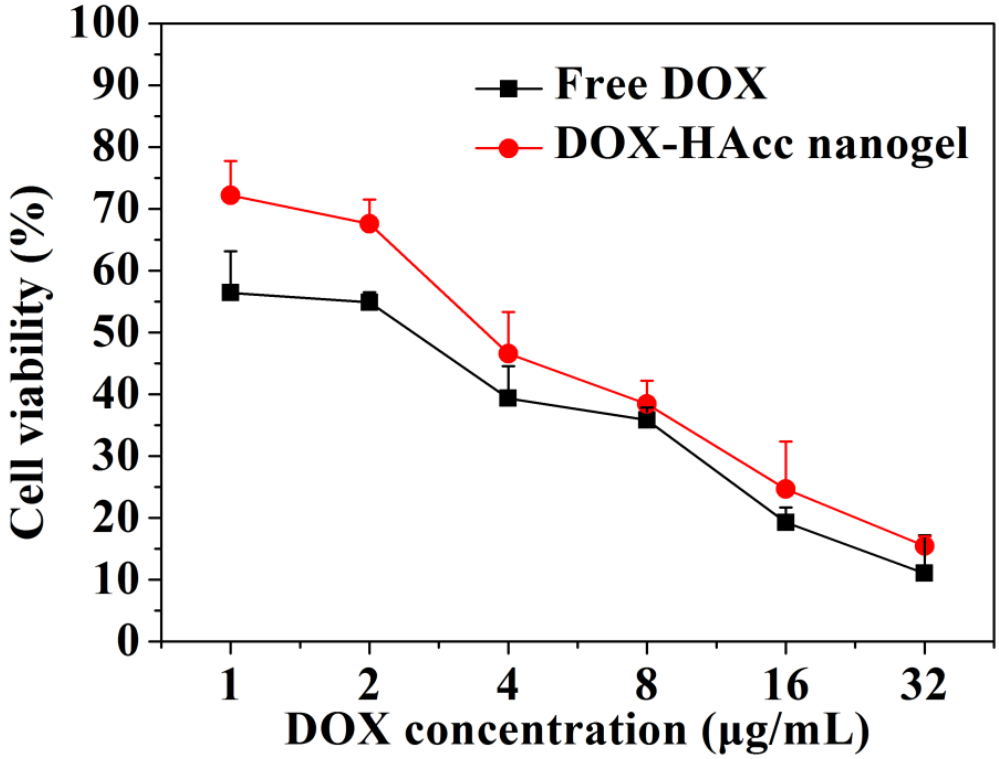

Fig. S7. The *in vitro* cytotoxicity of free DOX and DOX-loaded HAcc nanogels against LNCaP cell line (mean ± s.d., n = 3).

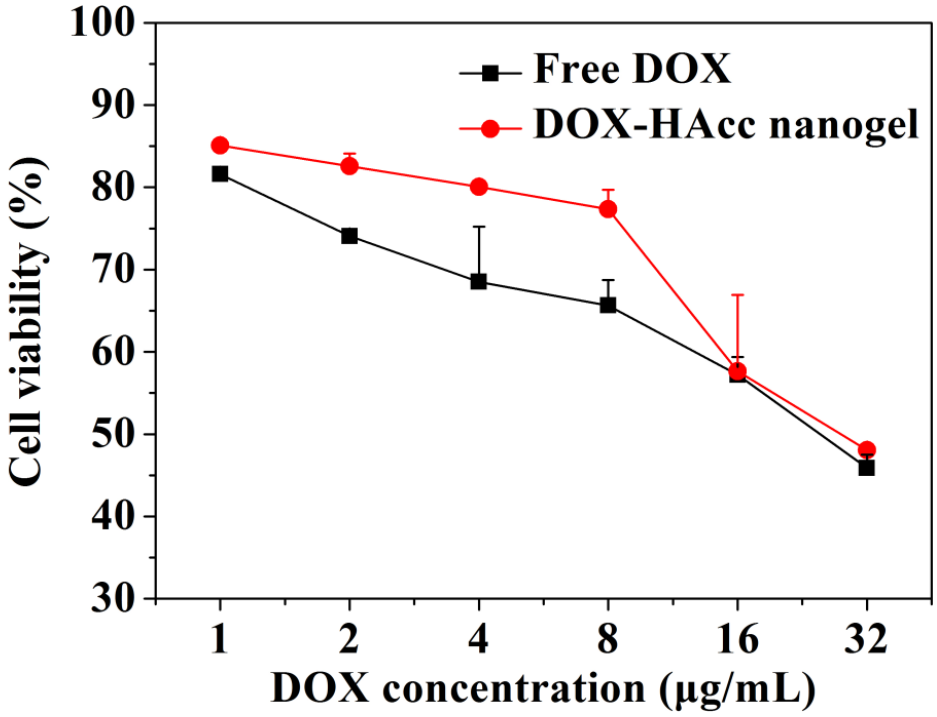

Fig. S8. The *in vitro* cytotoxicity of free DOX and DOX-loaded HAcc nanogels against H22 cell line (mean ± s.d., n = 3).

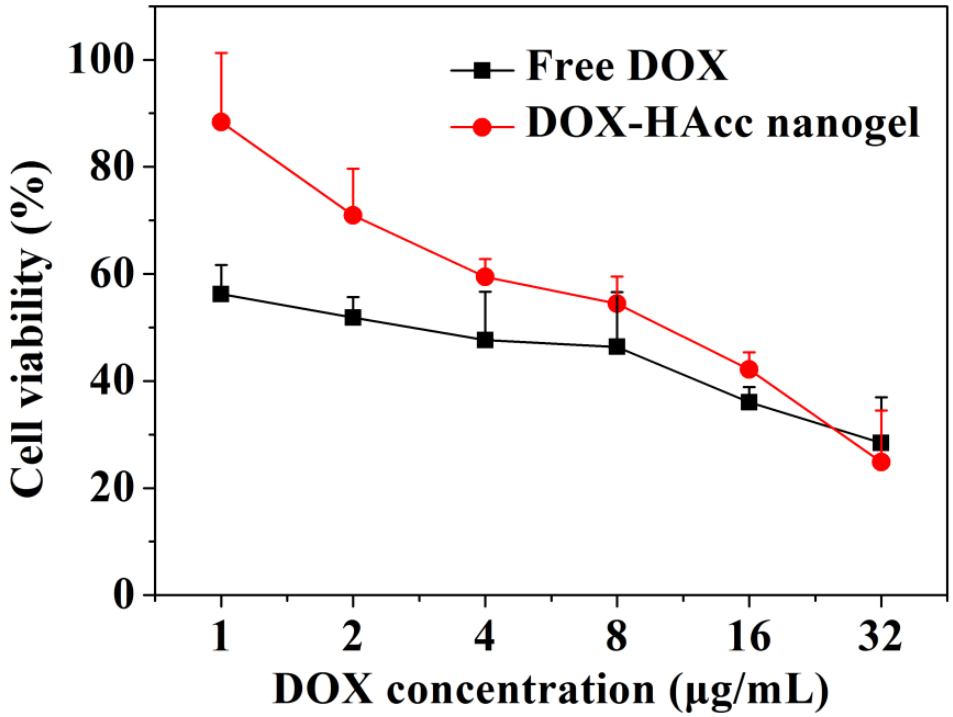

Fig. S9. The *in vitro* cytotoxicity of free DOX and DOX-loaded HAcc nanogels against A549 cell line (mean ± s.d., n = 3).

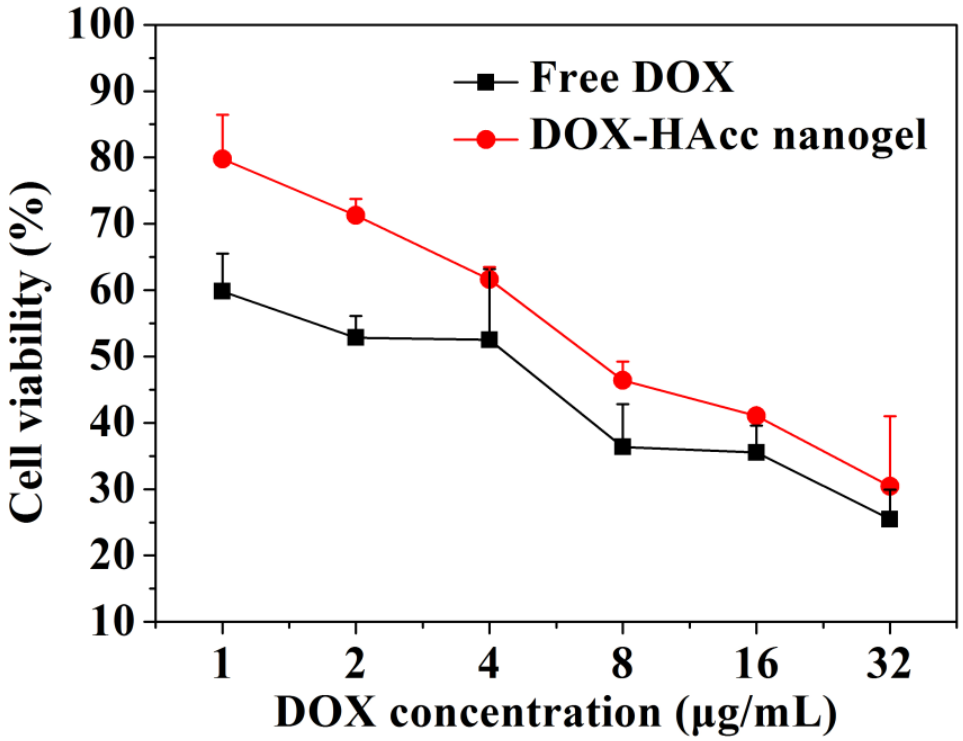

Fig. S10. The *in vitro* cytotoxicity of free DOX and DOX-loaded HAcc nanogels against NIH3T3 cell line (mean ± s.d., n = 3).

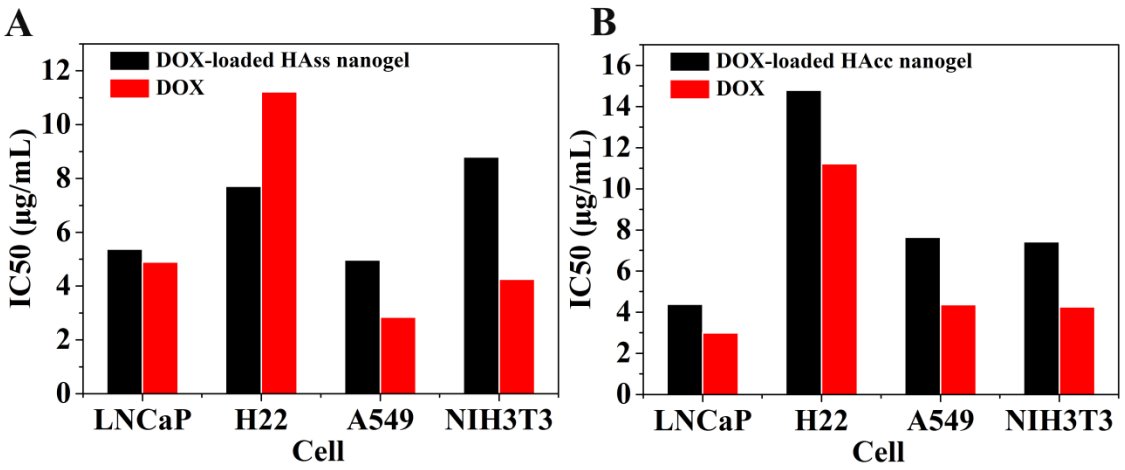

Fig. S11. The IC50 of DOX-loaded HAss nanogels (A) and DOX-loaded HAcc nanogels against four cell lines (mean ± s.d., n = 3). The MTT texts of DOX-loaded HAss nanogels and DOX-loaded HAcc nanogels are performed independently in LNCaP and A549 cells.

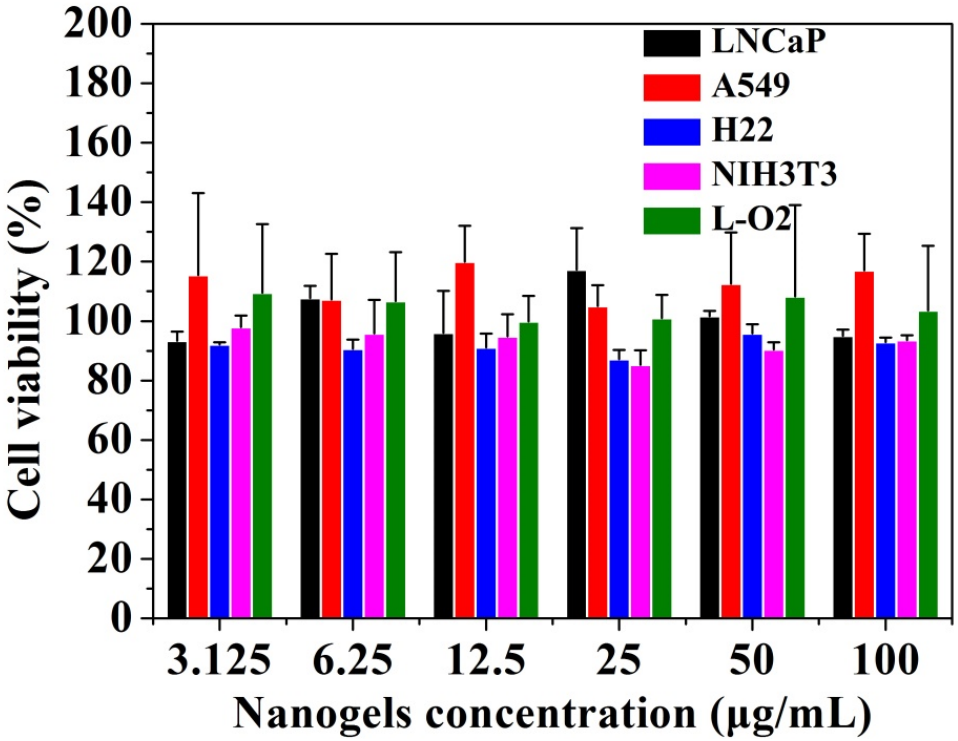

Fig. S12. The *in vitro* cytotoxicity of empty HAss against LNCaP, A549, H22, NIH3T3 and L-02 cell lines (mean ± s.d., n = 3).

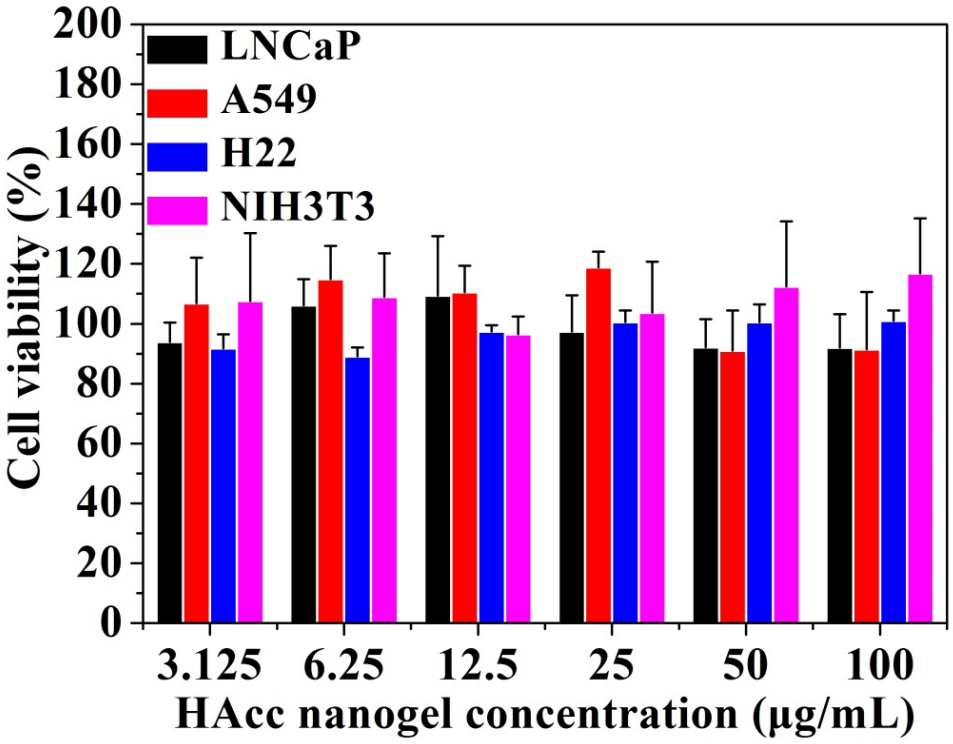

Fig. S13. The *in vitro* cytotoxicity of empty HAcc nanogels against LNCaP, A549, H22, NIH3T3 cell lines (mean ± s.d., n = 3).

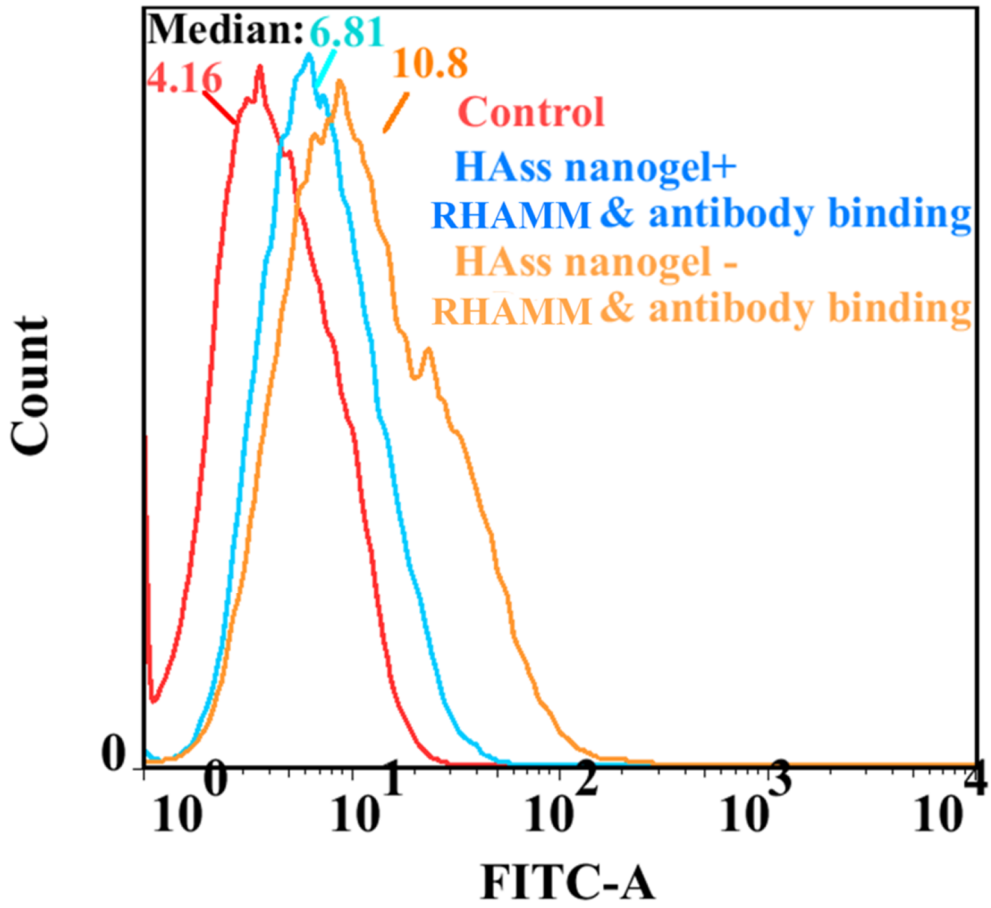

Fig. S14. Flow cytometry analysis plot of the binding capacity between RHAMM and anti-RHAMM antibody with (blue) or without (orange) the presence of HAss nanogels in LNCaP cells. The red line represents the control group.

Supplementary Data of Bio-Distribution of DOX-Loaded HAcc Nanogels

As a contrast, the distribution of DOX *in vivo* by intravenous (i.v.) injection with DOX-loaded HAcc nanogels (4.5 mg/kg DOX eq.) was detected in the same method as DOX-loaded HAcc nanogels group. As shown in Fig. S15, the enrichment amount of DOX in tumor is about 4%, which is more than that of free DOX. And the enrichment amount of DOX in heart is less than 4% and drop rapidly later, suggesting that the HAcc nanogel formulation also contributes to reducing the cardiotoxicity of DOX.

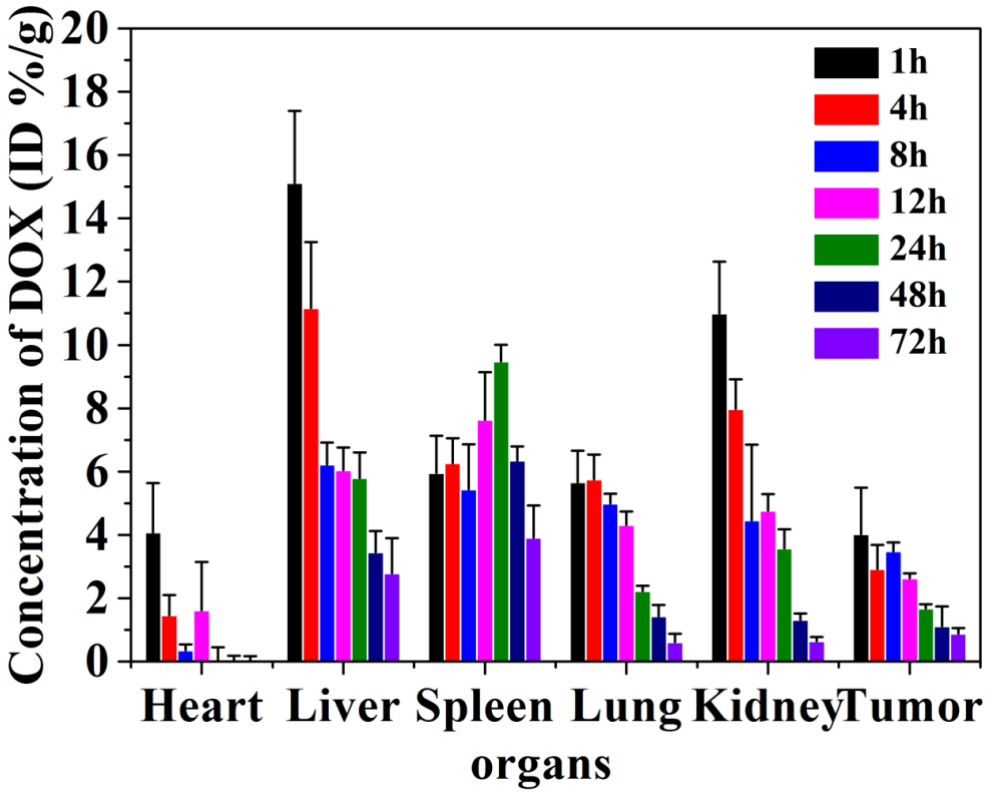

Fig. S15. Bio-distribution of DOX for DOX-loaded HAcc nanogels in H22 subcutaneous tumor-bearing mice. The values were presented as the percentage of ID per gram of collected organs (mean ± s.d., n = 3).

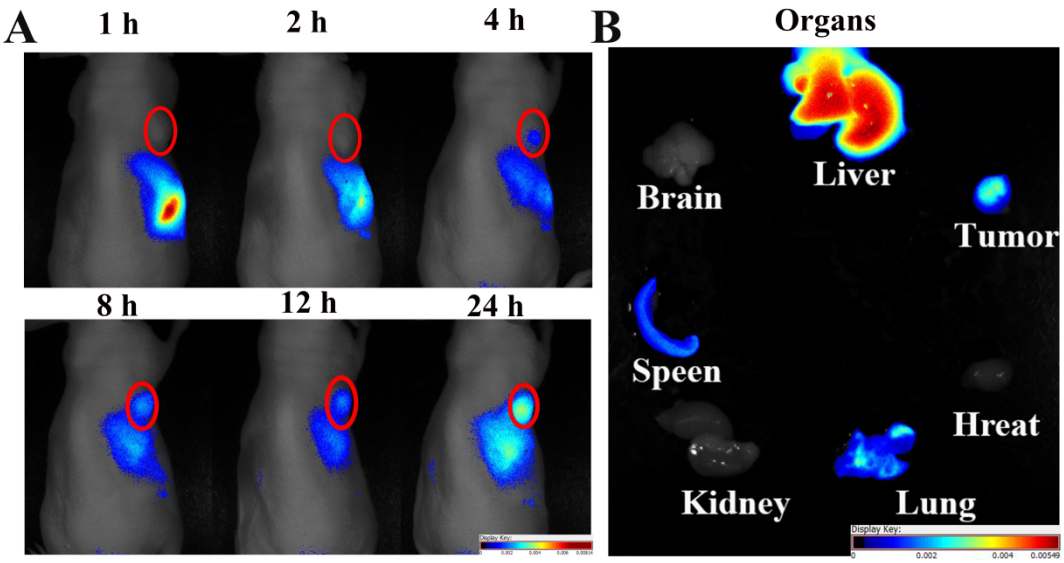

Fig. S16. (A) *In vivo* NIR fluorescence imaging of LNCaP tumor-bearing nude mice following i.v. injection of NIR-797 labeled HAss nanogels. The red circles are the location of LNCaP tumor. (B) *Ex vivo* NIR fluorescence image of organs at 24 h post-injection. The different fluorescence intensities are represented by different colors as shown in color histogram.

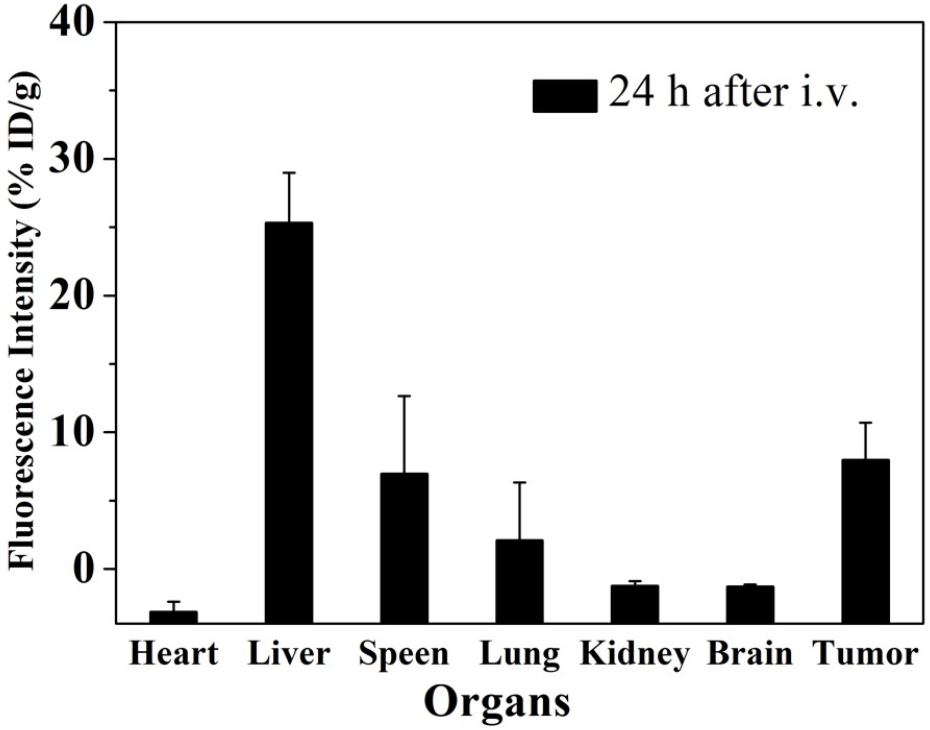

Fig. S17. Semi-quantitative statistics plot of *ex vivo* NIR fluorescence images at 24 h post-injection. The values were presented as the percentage of ID per gram of collected organs (mean ± s.d., n = 3).

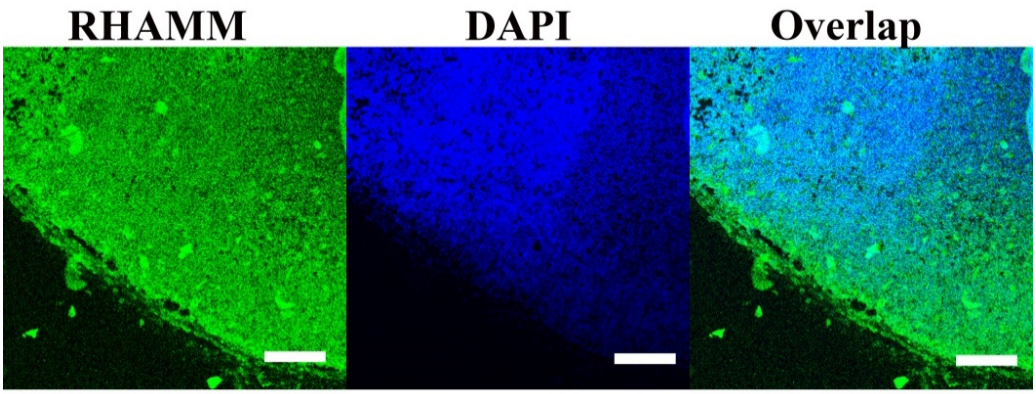

Fig. S18. Immunofluorescence staining sections of RHAMM (green) receptor expression in H22 metastatic lymph node (MLN). Nuclei were dyed by DAPI (blue). The scale bar is 100 μm.

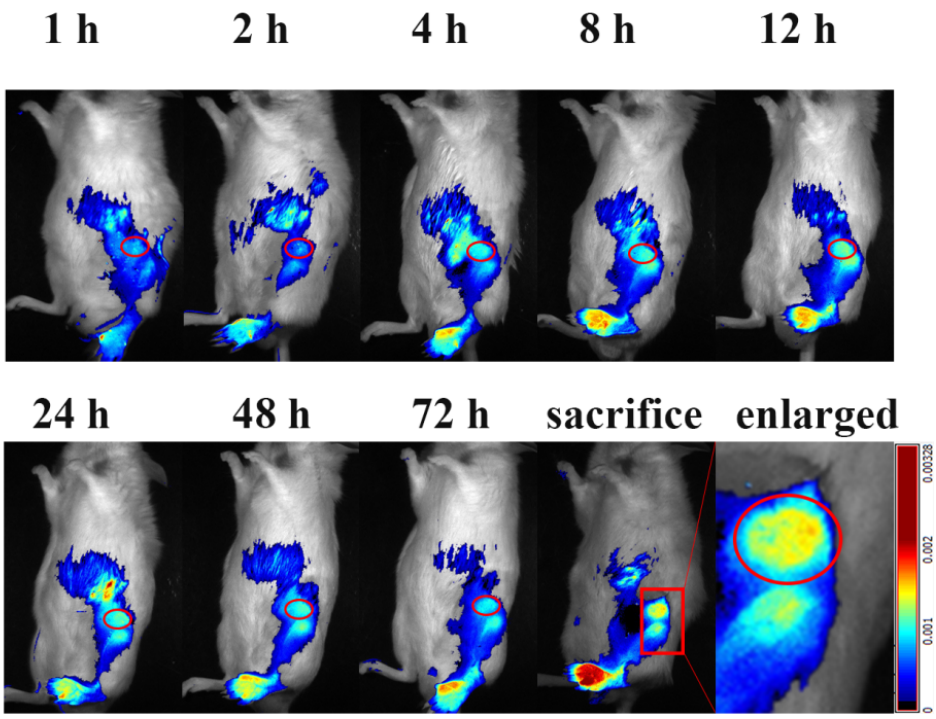

Fig. S19. *In vivo* NIR fluorescence imaging of H22 metastatic tumor-bearing mice following i.v. injection of NIR-797 labeled HAss nanogels. All data were normalized against 1 h post-injection. The red circles are the location of metastatic lymph nodes. The different fluorescence intensities are represented by different colors as shown in color histogram.

References

1. Lin C, Zhong Z, Lok MC, Jiang X, Hennink WE, Feijen J, Engbersen JFJ. Novel bioreducible poly(amido amine)s for highly efficient gene delivery. Bioconju Chem. 2007; 18: 138-145.

2. Wang J, Wu W, Zhang YJ, Wang X, Qian HQ, Liu BR, Jiang XQ. The combined effects of size and surface chemistry on the accumulation of boronic acid-rich protein nanoparticles in tumors. Biomaterials. 2014; 35: 866-878.